

Manuscript Number: APCATB-D-18-04366R1

Title: Development of visible-light-responsive morphology-controlled brookite TiO₂ nanorods by site-selective loading of AuAg bimetallic nanoparticles

Article Type: Research Paper

Keywords: Brookite; Surface plasmon resonance; AuAg bimetallic; Visible-light-responsive; Photocatalytic

Corresponding Author: Professor Teruhisa Ohno,

Corresponding Author's Institution: Kyushu Institute of Technology

First Author: Ying Ma

Order of Authors: Ying Ma; Katsuichiro Kobayashi; Yu Cao; Teruhisa Ohno

Development of visible-light-responsive morphology-controlled brookite TiO₂ nanorods by site-selective loading of AuAg bimetallic nanoparticles

Ying Ma ^a, Katsuichiro Kobayashi ^a, Yu Cao ^a, Teruhisa Ohno ^{a, b, *}

^a Department of Materials Science, Faculty of Engineering, Kyushu Institute of Technology, 1-1 Sensui-cho, Tobata-ku, Kitakyushu, Fukuoka, 804-8550, Japan

^b Research Center for Solar Light Energy Conversion, 1-1 Sensuicho, Tobata, Kitakyushu 804-8550, Japan

*E-mail: tohno@che.kyutech.ac.jp

Abstract

Morphology-controlled brookite TiO₂ nanorods loaded with AuAg bimetallic nanoparticles were synthesized by a facile photoreduction process to develop visible-light-responsive photocatalytic performance. The AuAg bimetallic nanoparticles provide good stability and excellent localized surface plasmon resonance (LSPR) effect. Moreover, the AuAg bimetallic nanoparticles were selectively deposited on the reduction facets of brookite TiO₂ nanorods, facilitating the charge separation. As expected, the as-prepared AuAg-TiO₂ nanorods showed enhanced visible light harvesting and decreased electron-hole recombination, resulting in superior visible-light-responsive photocatalytic performance. When the loading amount of AuAg nanoparticles was controlled at 0.5 wt%, the AuAg-TiO₂ nanorods yield 102 ppm acetone with visible-light irradiation

for 5 h, far exceeding than those of bare brookite TiO_2 nanorods.

Keywords: Brookite; Surface plasmon resonance; AuAg bimetallic; Visible-light-responsive; Photocatalytic

1. Introduction

Photocatalysts, especially titanium dioxide (TiO_2), have been extensively studied as promising materials for water splitting and decomposition of organic pollutants by using solar energy. TiO_2 typically exists as three types of polymorphs: anatase, rutile and brookite [1-3]. With the recent development of improved methods for synthesis of brookite TiO_2 , many investigations of its photocatalytic properties have been carried out. It has been shown that brookite TiO_2 is superior for photocatalytic reactions than those of anatase and rutile due to the appropriate depth of electron traps, which greatly benefits the overall photocatalytic activity [4-6]. However, the photoabsorption of brookite TiO_2 is limited to UV light as is rutile TiO_2 and anatase TiO_2 , which greatly hinders the utilization of solar energy and practical applications in photocatalytic decompositions especially indoors [7]. Therefore, it is critical to develop the visible-light response of brookite TiO_2 for photocatalysis by enhancing its ability to absorb and harvest visible light.

Surface plasmon resonances of metallic nanoparticles provide an efficient strategy for obtaining advanced photovoltaic and photocatalytic devices. As the most important and common co-catalysts, Ag and Au

have been studied extensively because of their LSPR effect on semiconductor photocatalysts, which could not only promote visible light absorption but also charge separation. For instance, an Ag-TiO₂ composite catalyst [8], Ag@TiO₂ nanorods [9], Au-TiO₂ [10] and Ag-TiO₂ plasmonic hybrid nanocomposites [11] have been prepared and shown greatly enhanced visible-light-responsive photocatalytic performance. However, pure Au nanoparticles exhibit low LSPR effect and Ag nanoparticles demonstrate poor stability under visible light. Hence, AuAg bimetallic nanoparticles attracted much attention due to the synergistic effect of Ag and Au, enabling good stability and excellent LSPR effect. Tahir et al. reported a synergistic effect of plasmonic Au/Ag alloy nanoparticles used for coating TiO₂ nanowires on visible-light-promoted photoreduction of CO₂ to fuels [12]. Huang's group validated the superiority of gold-silver-modified plasmonic photoanodes for solar cells with high efficiency under visible light [13]. Therefore, it is highly desirable to investigate the LSPR effect of AuAg bimetallic nanoparticles on brookite TiO₂, developing efficient visible-light-driven photocatalyst.

In this study, well-defined AuAg-brookite TiO₂ nanorods were fabricated by selectively loading AuAg bimetallic nanoparticles on morphology-controlled brookite TiO₂ nanorods. The efficient LSPR effect of AuAg nanoparticles on reduction facets of brookite TiO₂ nanorods

remarkably enhanced visible-light absorption and charge separation, thus improving visible-light-driven photocatalytic performance. The combination of Au and Ag enables not only superior LSPR activity but also good stability, making it an ideal material for modifying brookite TiO_2 nanorods. Furthermore, 0.5 wt% AuAg-brookite showed high level of acetone production for decomposition of 2-propenal under visible light illumination, which is about 3 and 4 times of those of 0.5 wt% Ag- TiO_2 and 0.5 wt% Au- TiO_2 . The results of this study provide insights for the development of efficient visible-light-responsive photocatalytic performance of brookite TiO_2 nanorods by introducing the LSPR effect of AuAg bimetallic nanoparticles.

2. Experimental section

2.1 Preparation of brookite TiO_2 nanorods

All of the chemical materials used in this study were analytical grade and used without further purification. The resistivity of the deionized water used in all of the reactions was 18.25 $\text{M}\Omega\cdot\text{cm}$. Brookite TiO_2 nanorods were prepared through a facial hydrothermal reaction according to a reported method [14]. Urea (21.02 g) was dissolved in titanium bis(ammonium lactate) dihydroxide (TALH, 5 mL) and deionized water (45 mL) with stirring for 2 hours. Then the uniform mixed solution was transferred into a Teflon cup and kept at 200 °C for 48 h. When the

autoclave had cooled down to room temperature, the samples were collected by centrifugation until the ionic strength of the filtrate was less than $10 \mu\text{S cm}^{-1}$. Finally, pure brookite TiO_2 nanorods could be obtained by drying at 60°C for 4 hours in a vacuum oven. To remove the organic compounds that may have remained or had been adsorbed on the surface of brookite TiO_2 nanorods, the products were irradiated with a 500 W mercury lamp (Ushio, SX-UI501UO) for 24 h. Commercial brookite TiO_2 was purchased from High Purity Materials Kojundo Chemical Laboratory Co. LTD.

2.2 Fabrication of AgAu/ TiO_2 nanorods

AgAu bimetallic nanoparticles were loaded on the as-prepared brookite TiO_2 nanorods through a photo-reduction method. Firstly, 0.4 g brookite TiO_2 nanorod was dispersed in distilled water (10 mL) and methanol (10 mL). Then the mixed solution was bubbled with nitrogen for 1 hour and irradiated with UV light (220 mW cm^{-2}). During the irradiation, 0.05 M silver nitrate was added at first. After 15 min, 0.029 M HAuCl_4 was added to the solution and its addition was repeated for 4 times. In order to control the loading amount of Au and Ag, the volume of added solution was regulated. More specifically, the loading amount of AuAg was confined to 0.25 wt%, 0.5 wt%, 0.75 wt% and 1.0 wt%, in which the molar ratio of Au and Ag is 1:1. For comparison, 0.5 wt% AgAu nanoparticles was also loaded on commercial brookite TiO_2 by the

same procedure.

2.3 Characterization

The crystalline phase of as-prepared samples was investigated by using a powder X-ray diffraction (XRD) instrument (MiniFlex II, Rigaku Co.). The morphologies and nanostructures of the samples were characterized by using a scanning electron microscope (SEM, JSM-6701FONO) and a transmission electron microscope (TEM, Hitachi, H-9000NAR, 200 kV). High-resolution TEM (HRTEM) images were obtained through a Tecnai G2 F30 S-TWIN (30 kV). The surface area of the samples were obtained from a Quantachrome Nova 4200e using the Brunauer-Emmett-Teller (BET) and Barrett-Joyner-Halenda (BJH) methods, respectively. UV-visible diffuse reflectance spectra showing the optical properties of samples were obtained by a UV-2500PC (Shimadzu) equipped with an integrating sphere unit. X-ray photoelectron spectra (XPS) were obtained by a Thermo ESCALAB 250Xi system at room temperature using Al K α with monochromatic radiation. Apparent quantum efficiency (AQE) at wavelengths from 400 to 600 nm was recorded by the ratio of acetone production and amount of incident photons by using a Xe lamp equipped with a band-pass filter (Asahi Spectra Co., Ltd.) centered at 400 nm, 450 nm, 470 nm, 500 nm, 550 nm and 600 nm. Photoluminescence (PL) spectra were characterized by the PF-8500 spectrometer using the excitation wavelength of 350 nm.

2.4 Photocatalytic test

The photocatalytic activity of the samples was evaluated by decomposition of 2-propanol in gas phase. The photocatalyst (200 mg) was spread on a glass dish (4 cm^2) and the glass dish was put into a Tedlar bag (AS ONE Co. Ltd.) with a volume of 125 mL mixed air (79% N_2 , 21% O_2 , $<0.1\text{ ppm}$ of CO_2 , 500 ppm of 2-propanol). Before visible-light irradiation, the photocatalyst was left in the dark for 1 hour to reach adsorption equilibrium. Then the photocatalyst was illuminated by visible light of 100 mW cm^{-2} (or 50 mW cm^{-2}) from a Xenon lamp equipped with a Yellow-44 filter. The concentration evolutions of 2-propanol, CO_2 and acetone during the photocatalytic process were determined by gas chromatography (Agilent/Inficon 3000 Micro GC) with a PLOT U column and OV-1 column.

3. Results and discussion

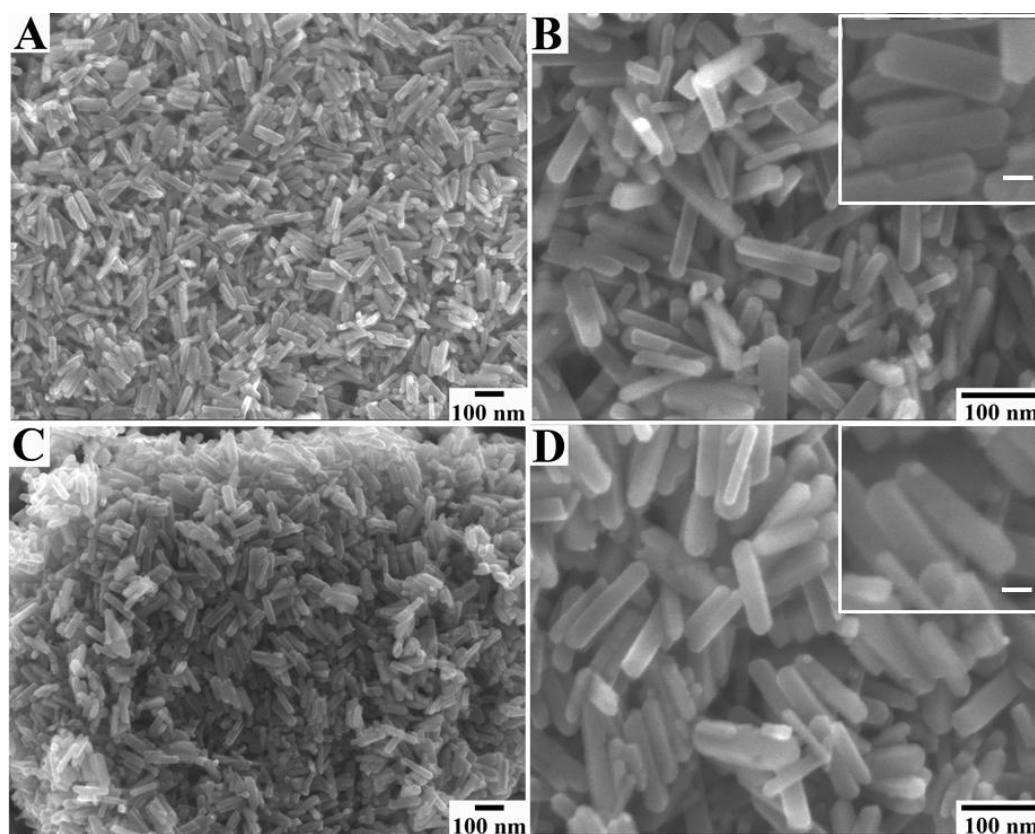


Fig. 1. SEM images of (A, B) pristine brookite TiO_2 (C, D) 0.5 wt% AuAg- TiO_2 nanorods. (The inset graphs are the corresponding enlarged SEM images and the scale bar represents 20 nm).

The nanorod shape of brookite TiO_2 is shown by SEM images in Figure 1. It can be clearly seen that ordered nanorods with lengths of about 110 nm and widths of 20 nm have smooth surfaces and triangular-like tips at the ends of the rods (Figure 1B). As reported previously, a nanorod shows a large $\{210\}$ crystal face and a small $\{212\}$ crystal face in the flank and top of brookite TiO_2 , corresponding to reduction and oxidation facets, respectively [15,16]. Moreover, the large proportion of reduction sites in as-prepared brookite TiO_2 provides

numerous active sites for photoreduction. As expected, the nanorod shape was preserved well and there were few nanoparticles distributed on the reduction facets of brookite TiO_2 nanorods after loading the AuAg nanoparticles as shown in Figure 1D.

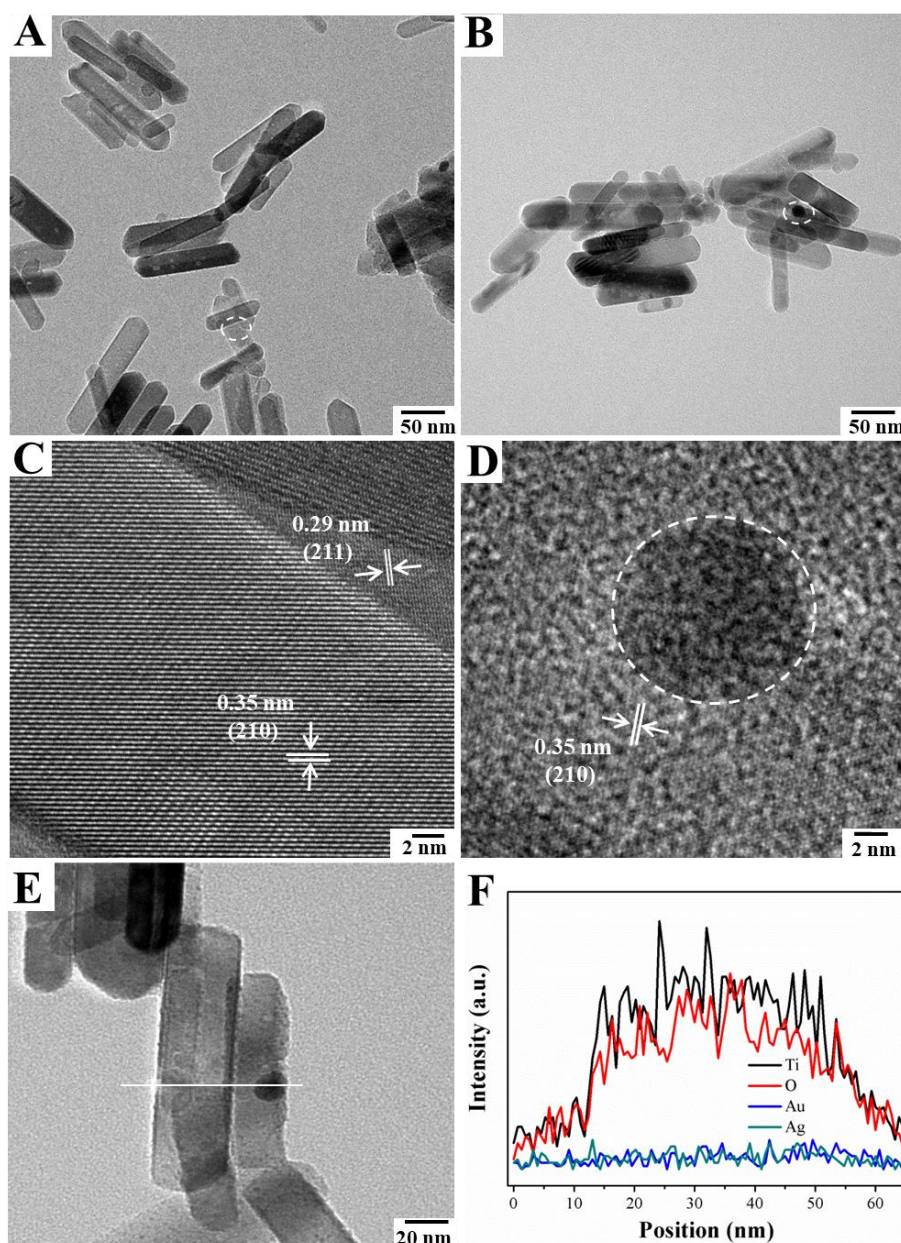


Fig. 2. TEM images of (A) pristine brookite TiO_2 and (B) 0.5 wt% AuAg- TiO_2 nanorods, HRTEM images of (C) pristine brookite TiO_2 and (D) 0.5 wt% AuAg- TiO_2 nanorods, (E) TEM image and (F) the

corresponding line-scan electron energy loss spectroscopy (EELS) of 0.5 wt% AuAg-TiO₂ nanorods.

The TEM images in Figure 2 show the specific morphology of pure brookite TiO₂ nanorods and the existence of nanoparticles in the modified brookite TiO₂ nanorods. The TEM image of samples shows a rod-like shape with a triangular end and a tetragonal brookite structure, being consistent with the SEM images. The spacing lattices of 0.35 nm and 0.29 nm in HRTEM image derived from the bare nanorods marked with dotted line circle in TEM image can be assigned to the (210) and (211) facets of brookite TiO₂, which are identified as the reduction and oxidation facets [14,15]. Most importantly, nanoparticles (marked with dotted line circle in Figure 2B and 2D) with diameters of about 10 nm are distributed on the (210) crystal plane. This also confirms that the (210) crystal plane of brookite TiO₂ nanorods provides reduction sites for depositing noble metals. The loaded AuAg nanoparticles on brookite TiO₂ nanorods were further confirmed by EELS (Figure 2F). It can be seen that Au and Ag have a fitted distribution on the characteristic nanorod shape of TiO₂, demonstrating that the AuAg bimetallic nanoparticles have been successfully located on the as-prepared TiO₂ nanorods.

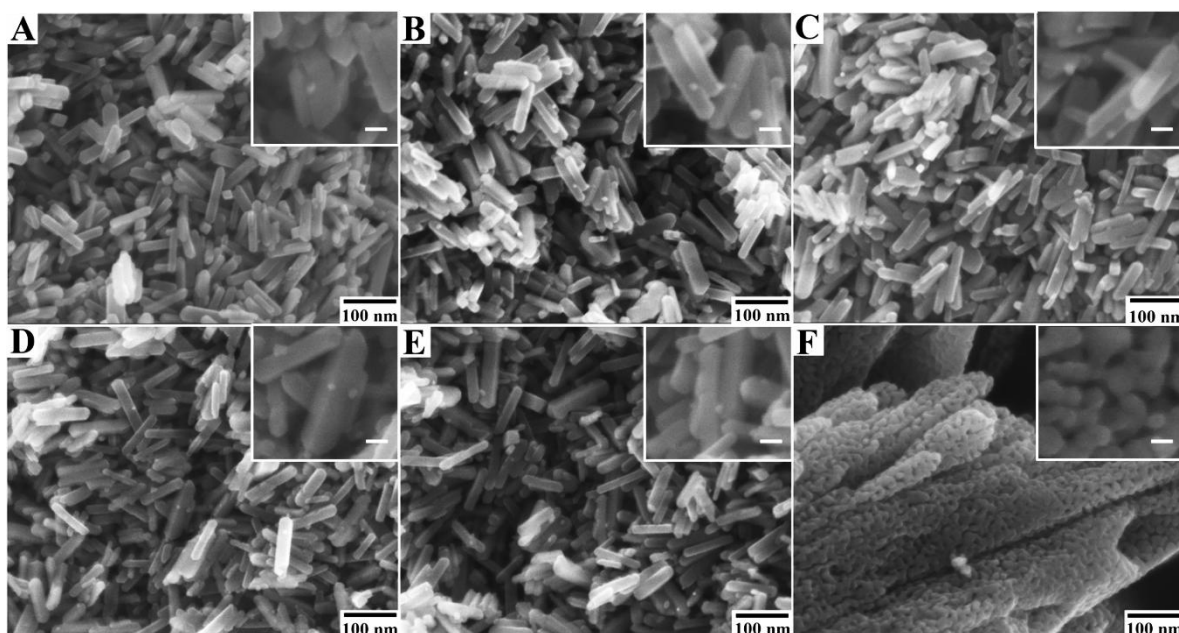


Fig. 3. SEM images of (A) 0.25 wt% AuAg-TiO₂ nanorods (B) 0.75 wt% AuAg-TiO₂ nanorods (C) 1.0 wt% AuAg-TiO₂ nanorods (D) 0.5 wt% Au-TiO₂ nanorods (E) 0.5 wt% Ag-TiO₂ nanorods (F) commercial brookite. (The inset graphs are the corresponding enlarged SEM images and the scale bar represents 20 nm).

The loading amount of AuAg on brookite TiO₂ nanorods can be theoretically regulated by controlling the volume of the precursor solution. With an increase in the loading amount of AuAg, the nanoparticles become more obvious in SEM images. As depicted, The AuAg nanoparticles can hardly be seen in 0.25 wt% AuAg-TiO₂ nanorods (Figure 3A) due to the relatively small loading amount. When the weight percentage of AuAg was increased to 0.5 wt%, a small amount of nanoparticles was distributed on the TiO₂ nanorods (Figure 1D). However, a large amount of nanoparticles was deposited on the nanorods for 0.75

wt% AuAg-TiO₂ and 1.0 wt% AuAg-TiO₂ nanorods. It is notable that all of the nanoparticles were distributed on the reduction facets of nanorods, suggesting that the photoreduction reaction occurred on a specific crystal plane with separation of the reduction and oxidation sites in the brookite TiO₂ nanorods. For comparison, pure 0.5 wt% Au-loaded brookite TiO₂ and 0.5 wt% Ag-loaded brookite TiO₂ nanorods were synthesized, and SEM images are shown in Figure 3. As in the case of 0.5 wt% AuAg-TiO₂, the Au-TiO₂ and Ag-TiO₂ nanorods had few nanoparticles on the reduction crystal planes of the nanorods. It was confirmed that pristine Au nanoparticles and Ag nanoparticles can be formed by photoreduction. For comparison, the SEM image of commercial brookite was also characterized. It is observed that commercial brookite is composed of stacked nanoparticles with diameter of nearly 20 nm.

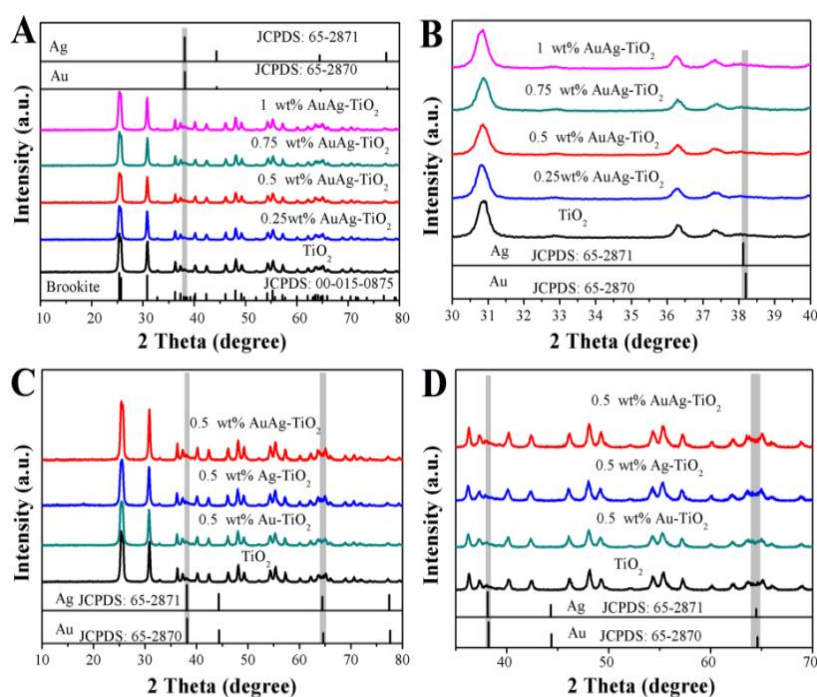


Fig. 4. XRD patterns (A and B) of AuAg-TiO₂ with different loading

amounts of AuAg and XRD patterns (C and D) of brookite TiO_2 loaded with 0.5 wt% of different metals.

The XRD patterns were characterized and are shown in Figure 4, revealing the crystalline structure and crystal phase of samples. The peaks of pure nanorods can be well indexed to brookite TiO_2 (JCPDS: 00-015-0875) [17,18] without other impurity peaks, indicating high purity. Furthermore, the samples with different loading amounts of AuAg exhibited peaks that agreed well with the pristine brookite TiO_2 nanorods and no peak of Au or Ag, which is thought to be due to the small amount and good dispersion of loaded metals on the brookite TiO_2 nanorods. Similarly, there was no sign of Au (JCPDS: 65-2870) and Ag (JCPDS: 65-2871) [19,20] in the as-prepared Au- TiO_2 and Ag- TiO_2 as shown in Figure 4C and 4D.

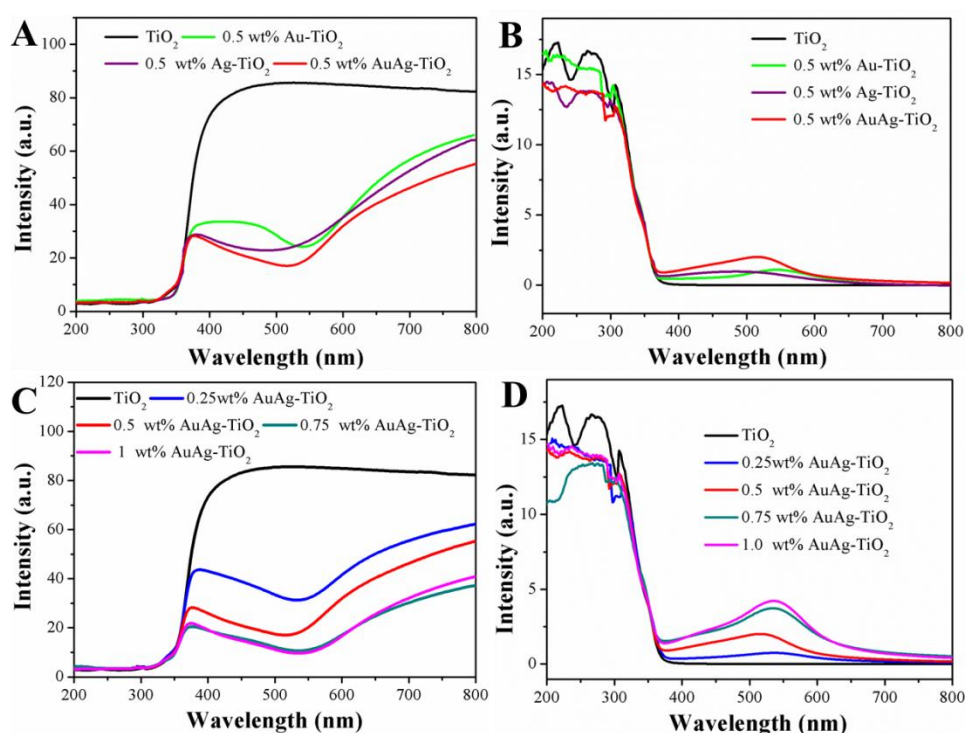


Fig. 5. UV-visible diffuse reflectance (DR) spectra (A) and UV-visible absorption spectra (B) of brookite TiO₂ and brookite TiO₂ loaded with 0.5 wt% of different metals and UV-visible DR (C) and UV-visible absorption spectra (D) of brookite TiO₂ and AuAg-TiO₂ with different loading amounts of AuAg.

The optical properties of TiO₂, Au-TiO₂, Ag-TiO₂ and AuAg-TiO₂ were revealed by the UV-visible DR and absorption spectra shown in Figure 5. The pure brookite TiO₂ shows an absorption edge at 380 nm in the UV light region, suggesting that pure brookite TiO₂ nanorods can not be excited by visible light. However, Au-TiO₂ and Ag-TiO₂ show absorption peaks at 547 and 467 nm, respectively, which are assigned to the LSPR effect of Au and Ag on brookite TiO₂ [21-24]. It is worth notable that the AuAg-TiO₂ nanorods showed absorption in a wide range of 400-600 nm due to the LSPR effect of both Au and Ag nanoparticles. This also implies that Au and Ag have a synergistic effect of LSPR for brookite TiO₂ nanorods and greatly improve the visible-light absorptivity. Moreover, visible-light absorption is enhanced with an increase in the loading amount of AuAg nanoparticles. Table 1 shows the BET surface areas of the as-prepared samples. The commercial brookite samples present surface area of 38.1 m² g⁻¹, which is much smaller than that of as-prepared brookite TiO₂ nanorods. It can be seen that brookite TiO₂ nanorods had a surface area of 77.3 m² g⁻¹, which provides numerous

active sites for loading the AuAg bimetallic nanoparticles and photocatalytic reaction. Moreover, the surface area of the samples showed a slight decrease with an increase in the loading amount of AuAg nanoparticles.

Table 1 BET surface areas of the samples.

Samples	Commercial TiO ₂	Brookite TiO ₂	0.25 wt% AuAg-TiO ₂	0.5 wt% AuAg-TiO ₂	0.75 wt% AuAg-TiO ₂	1.0 wt% AuAg-TiO ₂
BET (m ² /g)	38.1	77.3	77.2	75.9	73.8	72.1

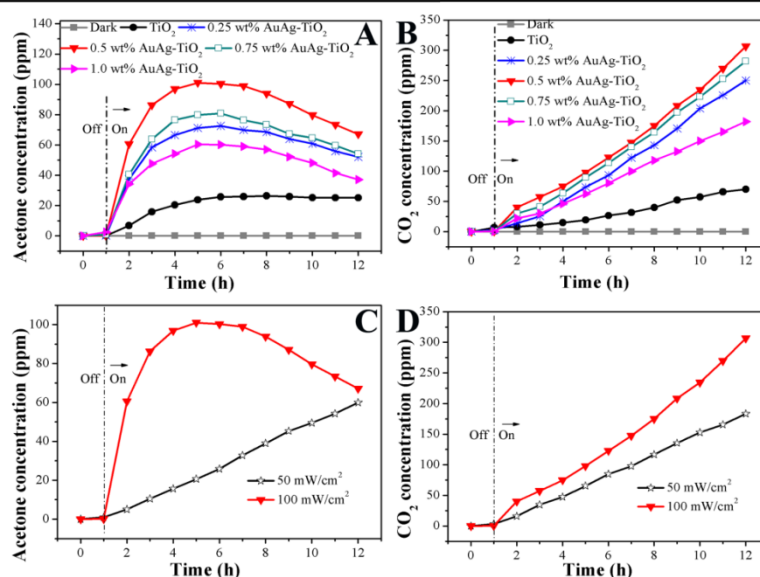


Fig. 6. Time courses of (A) acetone evolution and (B) CO₂ evolution from different photocatalysts and time courses of (C) acetone evolution and (D) CO₂ evolution from the 0.5 wt% AuAg-brookite TiO₂ under visible light with different light intensities.

To demonstrate the LSPR effect of AuAg bimetallic nanoparticles on the reduction facets of brookite TiO₂ nanorods, the photocatalytic activities of pristine brookite TiO₂ nanorods and AuAg-brookite TiO₂ nanorods for oxidation of 2-propanol were evaluated. Figure 6A and 6B show the time courses of acetone evolution and CO₂ evolution from

different photocatalysts under visible light illumination ($440 < \lambda < 800$ nm). It can be clearly seen that the brookite TiO_2 nanorods exhibited a weak visible-light-driven response and almost no photocatalytic performance under dark conditions. The weak visible-light-driven response is thought to be resulted from the defects in the as-obtained brookite TiO_2 nanorods. Both surface and bulk oxygen vacancies would have functions in the photo-reaction process. Light absorption of photocatalysts can be improved by surface and bulk oxygen vacancies. Furthermore, the surface oxygen vacancies promote charge separation, while the bulk vacancies act as recombination center of photogenerated electrons and holes [25,26]. As characterized by the UV-visible absorption spectra (Figure 5B), the as-prepared brookite TiO_2 shows no visible light absorption, indicating that the weak visible-light-driven photocatalytic response is mainly originated from the surface vacancies.

After loading AuAg bimetallic nanoparticles on the brookite TiO_2 nanorods, the photocatalytic properties were remarkably improved. The 0.5 wt% AuAg- TiO_2 nanorods showed the highest photocatalytic activity among the AuAg-loaded brookite TiO_2 nanorods tested, yielding 102 ppm of acetone when irradiated for 5 h with visible light. It is notable that the yield of acetone increased almost linearly over the 5-h period and then decreased due to the saturation of acetone on the surface of the photoatalysts and the decomposition from acetone to the final product,

CO₂ [27]. However, the acetone production of brookite TiO₂ nanorods is only 25 ppm even irradiated by visible light for 5 h. Similarly, the 0.5 wt% AuAg-TiO₂ nanorods showed the highest level of CO₂ production during the photocatalytic process. Based on these results, it was concluded that the amount of AuAg nanoparticles has an important effect on the surface plasmon-induced photocatalytic activity.

In addition, the photocatalytic activity of AuAg-TiO₂ was found to be strongly dependent on the light intensity as shown in Figure 6C and 6D. The acetone evolution in the case of illumination by visible light with intensity of 50 mW cm⁻² showed a linear increase with extension of time to 12 h, indicating that the yield of acetone did not reach saturation during the photocatalytic process. In contrast, the saturated production of acetone can be obtained at 6 h in the case of 100 mW cm⁻² visible light irradiation. However, it should be noted that the CO₂ production over the 12-h period showed a linear increase with an increase of visible light intensity. The results suggested that the photocatalytic performance is triggered by photocatalytic oxidation over AuAg nanoparticles or the thermal effect related to photoabsorption of incident light.

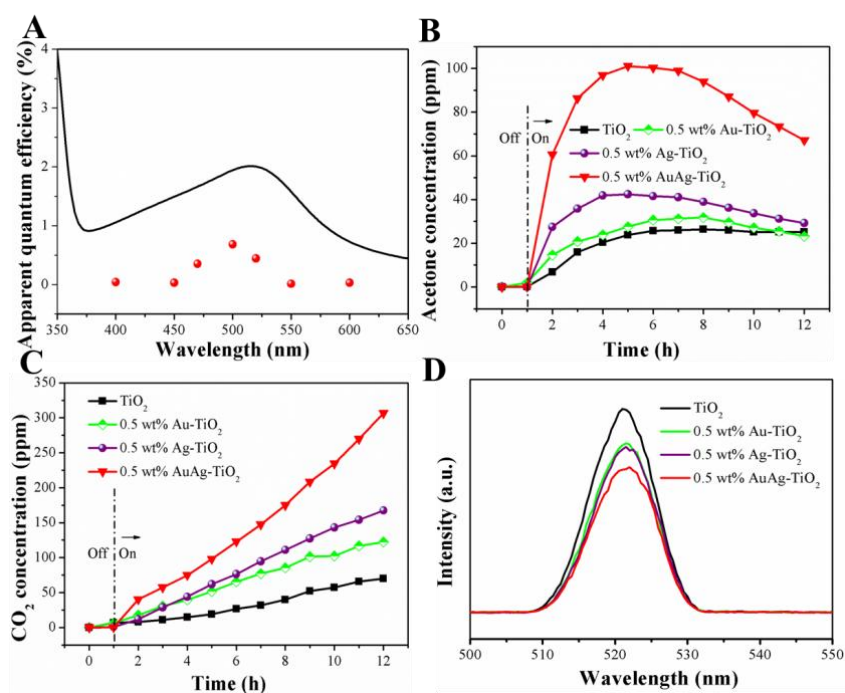


Fig. 7. (A) Action spectrum of acetone evolution from 2-propanol decomposition over 0.5 wt% AuAg-brookite TiO₂ nanorods together with Kubelka-Munk functions, time courses of (B) acetone evolution and (C) CO₂ evolution from Ag-TiO₂, Au-TiO₂ and AuAg-TiO₂ and (D) photoluminescence (PL) spectra of samples.

An action spectrum was obtained to reveal the factor determining the photocatalytic reaction and LSPR induced visible light responsibility of AuAg-TiO₂ nanorods. An AQE plot (Figure 7A) of AuAg-TiO₂ corresponds well to the Kubelka-Munk function, indicating that the photocatalytic behavior is induced by photoabsorption based on the LSPR effect of Au and Ag nanoparticles [28]. For comparison, the photocatalytic properties of pure Ag-TiO₂ and Au-TiO₂ were investigated to confirm the superiority of AuAg bimetallic nanoparticles. As demonstrated in Figure 7B and 7C, 0.5 wt% AuAg-TiO₂ showed

remarkably higher production levels of acetone and CO₂ than those of 0.5 wt% Au-TiO₂ and 0.5 wt% Ag-TiO₂. Moreover, the Au-TiO₂ nanorods showed the lowest photocatalytic activity among the samples tested, indicating a weak LSPR effect of Au nanoparticles on photocatalytic performance [29]. The acetone production derived by 0.5 wt% AuAg-TiO₂ is about 3 and 4 times of those of 0.5 wt% Ag-TiO₂ and 0.5 wt% Au-TiO₂, respectively. It has been proposed that the introduction of Au into Ag can greatly enhance the stability of Ag nanoparticles as well as preserve the high activity, which would provide an excellent LSPR effect [30].

Besides the enhanced visible light absorption of AuAg-TiO₂ verified by UV-visible absorption spectra, the PL intensities (Figure 7D) of TiO₂ and metal loaded TiO₂ were measured to investigate the charge separation efficiency. The PL emission located at about 520 nm corresponds to the charge transfer transition of trapped electrons in oxygen vacancy and plasma particles [31,32]. As the PL emission is a result of recombination of electrons and holes, the quenching of photoluminescence validates the efficient charge separation. It is well observed that the modified brookite TiO₂ nanorods exhibit decreased PL peak intensity, confirming enhanced charge separation by metal deposition. More specifically, 0.5 wt% AuAg-TiO₂ nanorods showed higher charge separation efficiency than those of TiO₂, Au-TiO₂ and Ag-TiO₂ samples being consistent with the

excellent photocatalytic performance under visible light irradiation. Moreover, Au-TiO₂ showed a much higher recombination rate of electrons and holes than that of Ag-TiO₂, indicating a weaker LSPR effect of Au nanoparticles than that of Ag nanoparticles on brookite TiO₂ nanorods. Based on these result, it is concluded that the combination of Au and Ag could provide a strong LSPR effect as well as stable Ag under visible light illumination, enabling the transfer of excited electrons from AuAg nanoparticles to the conduction band of TiO₂. As a result, the charge separation of AuAg-TiO₂ was greatly enhanced, being closely related to the photocatalytic activity.

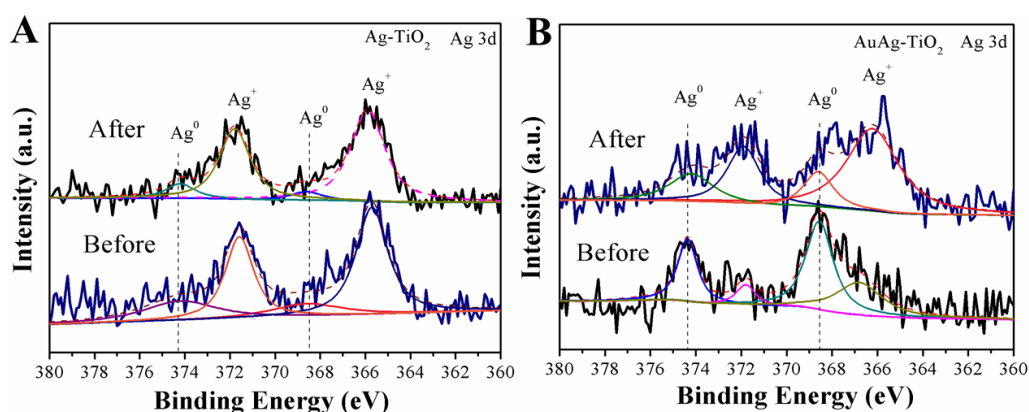


Fig. 8. 3d XPS patterns of (A) 0.5 wt% Ag-brookite TiO₂ and (B) 0.5 wt% AuAg-brookite TiO₂ before and after the photodecomposition process.

In order to confirm the valence states of Ag, XPS measurements were performed on Ag-TiO₂ and 0.5 wt% AuAg-TiO₂ before and after photocatalytic tests (Figure 8). For 0.5 wt% Ag-TiO₂ nanorods, the Ag 3d XPS pattern showed binding energies of Ag at 374.2 eV and 368.6 eV and binding energies of Ag⁺ at 365.8 eV and 371.8 eV, confirming the

co-existence of Ag and Ag₂O [27,33]. Furthermore, the binding energy peak of Ag⁺ was much higher than that of Ag, suggesting that Ag had been greatly oxidized before utilization. After photodecomposition, the peaks of Ag decreased and the binding energies of Ag 3d_{5/2} and Ag 3d_{3/2} of Ag⁺ at 365.8 eV and 371.8 eV in the 3d XPS pattern exhibit strong intensities, indicating that the pure Ag nanoparticles were highly unstable and oxidized during the photocatalytic process. However, the Ag 3d XPS spectra of 0.5 wt% AuAg-TiO₂ nanorods showed great differences from those of 0.5 wt% Ag-TiO₂. The Ag 3d XPS pattern of 0.5 wt% AuAg-TiO₂ before the photocatalytic test showed strong peaks of Ag at about 374.2 eV and 368.6 eV and weak peaks of Ag⁺, suggesting that AuAg bimetallic metals benefit the stability of Ag. On the other hand, the binding energy peak of Ag⁺ increased greatly after the photocatalytic test, indicating that Ag was partially oxidized during the photocatalytic reaction [34]. These results suggest that Ag is easily oxidized in the process of photocatalytic reaction.

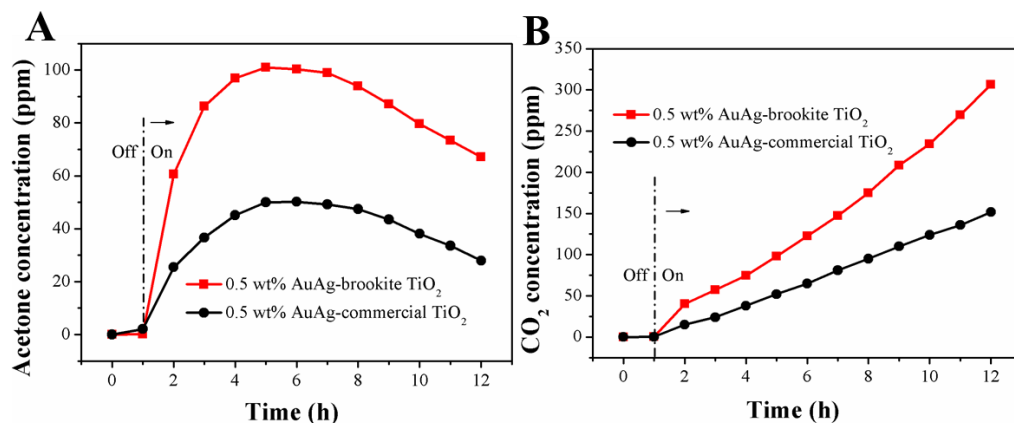


Fig. 9. Time courses of (A) acetone evolution and (B) CO₂ evolution derived from AuAg-commercial TiO₂ and AuAg-brookite TiO₂.

Apart from the advantages of AuAg bimetallic nanoparticles, control of the morphology of brookite TiO₂ nanorods contributes to the high photocatalytic performance, as was confirmed by a comparison of photocatalytic activities of 0.5 wt% AuAg-brookite TiO₂ and 0.5 wt% AuAg-commercial brookite TiO₂ (Figure 9). It should be mentioned that the production levels of acetone and CO₂ derived from the AuAg-commercial brookite TiO₂ were only about half of those generated over AuAg-brookite TiO₂. It is thought that selective loading of AuAg bimetallic nanoparticles on the reduction sites of brookite TiO₂ effectively promote charge separation and the large surface area of brookite nanorods (Table 1) furnishes numerous active sites, which are responsible for the superior photocatalytic activity. More specifically, the photogenerated electrons are transferred from AuAg nanoparticles to the reduction sites of brookite TiO₂ nanorods and take part in the reduction process, decreasing the recombination of electrons and holes. However, AuAg

nanoparticles are deposited randomly on commercial brookite TiO_2 particle and then the photogenerated electrons move from AuAg to brookite TiO_2 under visible-light irradiation. The mixed electrons and holes in AuAg-commercial TiO_2 would increase the recombination rate, leading to low photocatalytic activity.

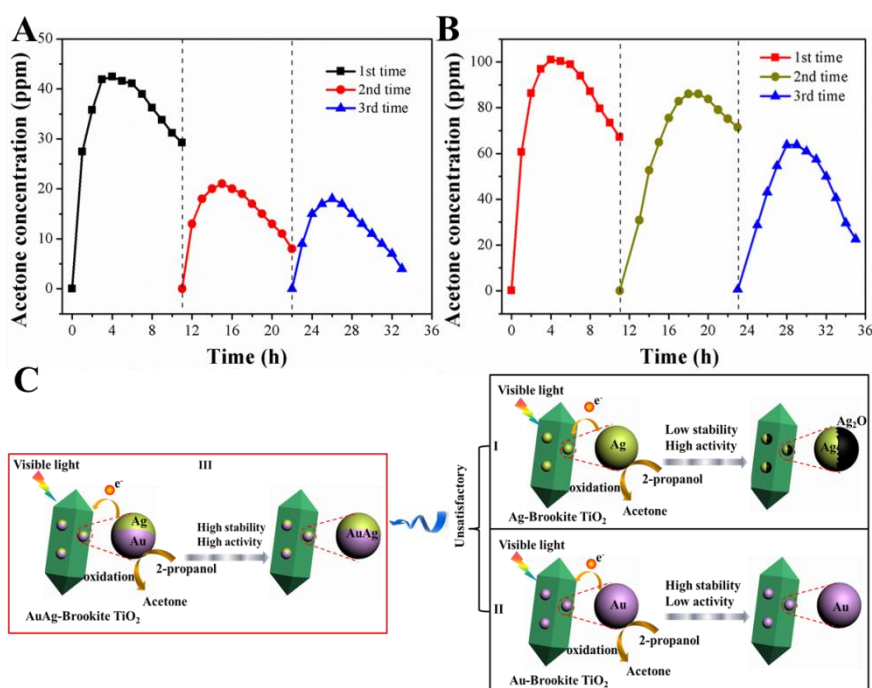


Fig. 10. Cyclic performance of (A) 0.5 wt% Ag-TiO₂ nanorods and (B) 0.5 wt% AuAg-TiO₂ nanorods for acetone production under visible light irradiation (C) illustration scheme for characteristics of as-prepared photocatalysts.

The cycling stabilities of the 0.5 wt% Ag-TiO₂ nanorods and 0.5 wt% AuAg-TiO₂ are shown in Figure 10. Cycling stability is an important factor for practical applications of photocatalysts. Notably, acetone evolution from 0.5 wt% Ag-TiO₂ showed a significant decrease at the second photocatalytic application compared to that in the initial

photocatalytic test. Moreover, a comparison of the decay efficiencies of photocatalytic activity of AuAg-TiO₂ and Ag-TiO₂ confirmed the superiority of AuAg-loaded brookite TiO₂ nanorods. After 3 cycles, the photocatalytic efficiency of 0.5 wt% Ag-TiO₂ had decreased to 41.2% of that in the initial test. However, the acetone production over 0.5 wt% AuAg-TiO₂ nanorods was as high as 64 ppm at 5 h after 3 cycles, which was 62.7% of the initial production, indicating that AuAg bimetallic nanoparticles are effective and stable during the photocatalytic reaction [35]. Based on the above results, it can be concluded that the introduction of Au into Ag nanoparticles effectively enhances the photocatalytic stability. As shown in Figure 10C, Ag and Au nanoparticles provide photogenerated electrons to brookite TiO₂ under visible light. The photogenerated electrons directly participate in the reduction reaction and the holes left in the metals participate in the oxidation reaction, enabling efficient charge separation. Since the Ag nanoparticles are easily to be oxidized to Ag₂O during the photocatalytic process, the photocatalytic stability of Ag-TiO₂ is unsatisfactory. As Au nanoparticles have good stability and a weak LSPR effect, the combination of Au and Ag would provide good stability and a high level of activity.

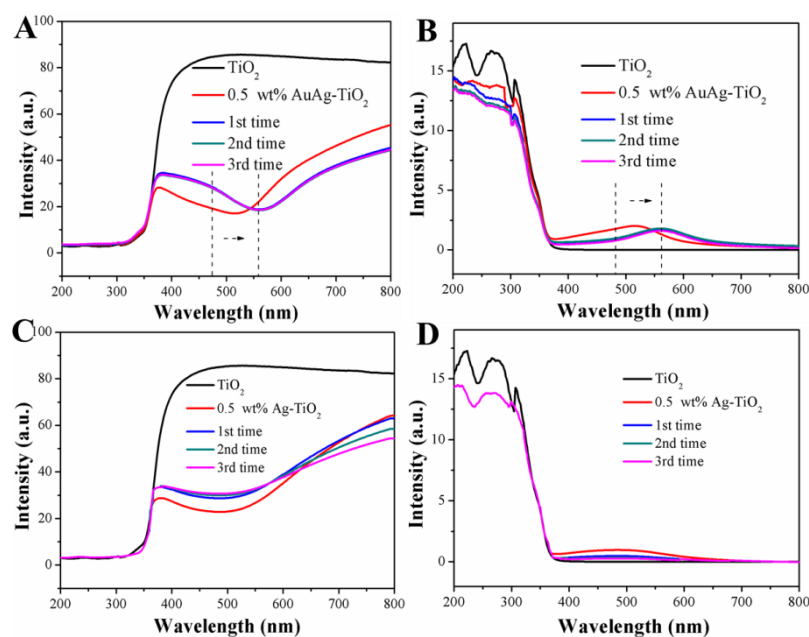


Fig. 11. UV-visible DR spectra (A) and UV-visible absorption spectra (B) of AuAg-TiO₂ with 3 photocatalytic tests and UV-visible DR spectra (C) and UV-visible absorption spectra (D) of Ag-TiO₂ with 3 photocatalytic tests.

UV-visible DR and absorption spectra (Figure 11) of AuAg-TiO₂ and Ag-TiO₂ after photocatalytic cycling tests were obtained to confirm the aforementioned proposal. For AuAg-TiO₂, the absorption peak showed a red shift in the first photocatalytic test and almost no change in the second and third photocatalytic tests. The obvious red-shift of absorption peak is proposed to be devoted to the partial oxidation of Ag during the photocatalytic reaction, which has been confirmed by the Ag 3d XPS pattern as shown in Figure 8. Importantly, the intensity of the absorption peak derived from the LSPR effect showed a slight decrease after photocatalytic cycling characterization that is related to the good

photocatalytic stability. However, the LSPR effect of Ag-TiO₂ showed a significant decrease after the photocatalytic process, corresponding to the oxidation of Ag nanoparticles. After 3 photocatalytic tests, Ag in TiO₂-Ag has had been greatly oxidized due to the weak absorption in the visible light range, being consistent with the low level of photocatalytic activity. It was confirmed that the design of AuAg nanoparticles could effectively facilitate the stability of Ag nanoparticles and high photocatalytic performance.

4. Conclusion

In summary, AuAg nanoparticles were photoreduced on the reduction crystal planes of brookite TiO₂ nanorods, greatly promoting visible-light-induced photocatalytic activities. The selectively deposited AuAg bimetallic nanoparticles provide not only a strong LSPR effect but also good stability, resulting in excellent photocatalytic performance of AuAg-TiO₂ nanorods for decomposition of 2-propanol. By regulating the amount of loaded AuAg nanoparticles, a significantly high level of photocatalytic activity could be obtained by 0.5 wt% AuAg-TiO₂ nanorods. This strategy offers an effective method for developing visible-light-responsive photocatalysts as well as for investigating the LSPR effect of AuAg bimetallic nanoparticles on brookite TiO₂ nanorods.

References

[1] L.X. Zheng, S.C. Han, H. Liu, P.P. Yu, X.S. Fang, Hierarchical

MoS₂ nanosheet@TiO₂ nanotube array composites with enhanced photocatalytic and photocurrent performances, *Small* 12 (2016) 1527–1536. <https://doi.org/10.1002/sml.201503441>.

[2] F. Iskandar, A.B.D. Nandiyanto, K.M. Yun, C.J. Hogan, J.K. Okuyama, P. Biswas, Enhanced photocatalytic performance of brookite TiO₂ macroporous particles prepared by spray drying with colloidal templating, *Adv. Mater.* 19 (2007) 1408–1412. <https://doi.org/10.1002/adma.200601822>.

[3] K. Maeda, N. Murakami, T. Ohno, Dependence of activity of rutile titanium(IV) oxide powder for photocatalytic overall water splitting on structural properties, *J. Phys. Chem. C* 118 (2014) 9093–9100. <https://pubs.acs.org/doi/abs/10.1021/jp502949q>.

[4] J.J.M. Vequizo, H. Matsunaga, T. Ishiku, S. Kamimura, T. Ohno, A. Yamakata, Trapping-induced enhancement of photocatalytic activity on brookite TiO₂ powders: comparison with anatase and rutile TiO₂ powders, *ACS Catal.* 7 (2017) 2644–2651. <https://pubs.acs.org/doi/abs/10.1021/acscatal.7b00131>.

[5] L.J. Liu, H.L. Zhao, J.M. Andino, Y. Li, Photocatalytic CO₂ reduction with H₂O on TiO₂ nanocrystals: comparison of anatase, rutile, and brookite polymorphs and exploration of surface chemistry, *ACS Catal.* 2 (2012) 1817–1828. <https://pubs.acs.org/doi/abs/10.1021/cs300273q>.

[6] J.F. Zhang, P. Zhou, J.J. Liu, J.G. Yu, New understanding of the

difference of photocatalytic activity among anatase, rutile and brookite TiO₂, Phys. Chem. Chem. Phys. 16 (2014) 20382–20386. <https://pubs.rsc.org/en/content/articlelanding/2014/cp/c4cp02201g>.

[7] K. Li, B.S. Peng, J.P. Jin, L. Zan, T.Y. Peng, Carbon nitride nanodots decorated brookite TiO₂ quasi nanocubes for enhanced activity and selectivity of visible-light-driven CO₂ reduction, Appl. Catal. B: Environ. 203 (2017) 910–916. <https://doi.org/10.1016/j.apcatb.2016.11.001>.

[8] M.X. Xu, Y.H. Wang, J.F. Geng, D.W. Jing, Photodecomposition of NO_x on Ag/TiO₂ composite catalysts in a gas phase reactor, Chem. Eng. J. 307 (2017) 181–188. <https://doi.org/10.1016/j.cej.2016.08.080>.

[9] K.K. Paul, P.K. Giri, Role of surface plasmons and hot electrons on the multi-step photocatalytic decay by defect enriched Ag@TiO₂ nanorods under visible light, J. Phys. Chem. C 121 (2017) 20016–20030. <https://pubs.acs.org/doi/abs/10.1021/acs.jpcc.7b05328>.

[10] M. Zhao, H. Xu, S.X. Quyang, H. Tong, H.Y. Chen, Y.X. Li, L.Z. Song, J.H. Ye, Fabricating a Au@TiO₂ plasmonic system to elucidate alkali-induced enhancement of photocatalytic H₂ evolution: surface potential shift or methanol oxidation acceleration, ACS Catal. 8 (2018) 4266–4277. <https://pubs.acs.org/doi/abs/10.1021/acscatal.8b00317>.

[11] H.L. Ran, J.J. Fan, X.L. Zhang, J. Mao, G.S. Shao, Enhanced performances of dye-sensitized solar cells based on Au-TiO₂ and Ag-TiO₂ plasmonic hybrid nanocomposites, Appl. Surf. Sci. 430 (2018)

415–423. <https://doi.org/10.1016/j.apsusc.2017.07.107>.

[12] M. Tahir, B. Tahir, N.A.S. Amin, Synergistic effect in plasmonic Au/Ag alloy NPs co-coated TiO₂NWs toward visible-light enhanced CO₂ photoreduction to fuels, *Appl. Catal. B: Environ.* 204 (2017) 548–560. <https://doi.org/10.1016/j.apcatb.2016.11.062>.

[13] S.P. Lim, Y.S. Lim, A. Pandikumar, H.N. Lim, Y.H. Ng, R. Ramaraj, D.C.S. Bien, Q.K. Abou-Zied, N.M. Huang, Gold–silver@TiO₂ nanocomposite-modified plasmonic photoanodes for higher efficiency dye-sensitized solar cells, *Phys. Chem. Chem. Phys.* 19 (2017) 1395–1407.

<https://pubs.rsc.org/en/content/articlelanding/2017/cp/c6cp05950c>.

[14] T. Ohno, T. Higo, H. Saito, S.S. Yuajn, Z.Y. Jin, Y. Yang, T. Tsubota, Dependence of photocatalytic activity on aspect ratio of a brookite TiO₂ nanorod and drastic improvement in visible light responsibility of a brookite TiO₂ nanorod by site-selective modification of Fe³⁺ on exposed faces, *J. Mol. Catal. A: Chem.* 396 (2015) 261–267. <https://doi.org/10.1016/j.molcata.2014.09.036>.

[15] T. Ohno, T. Higo, N. Murakami, H. Saito, Q.T. Zhang, Y. Yang, T. Tsubota, Photocatalytic reduction of CO₂ over exposed-crystal-face-controlled TiO₂ nanorod having a brookite phase with co-catalyst loading, *Appl. Catal. B: Environ.* 152–153 (2014) 309–316. <https://doi.org/10.1016/j.apcatb.2014.01.048>.

- [16] M. Choi, J.H. Lim, M. Baek, W. Choi, W. Kim, K. Yong, Investigating the unrevealed photocatalytic activity and stability of nanostructured brookite TiO₂ film as an environmental photocatalyst, *ACS Appl. Mater. Interfaces* 9 (2017) 16252–16260. <https://pubs.acs.org/doi/abs/10.1021/acsami.7b03481>.
- [17] M. Bellardita, A.D. Paola, B. Megna, L. Palmisano, Absolute crystallinity and photocatalytic activity of brookite TiO₂ samples, *Appl. Catal. B: Environ.* 201 (2017) 150–158. <https://doi.org/10.1016/j.apcatb.2016.08.012>.
- [18] S.Y. Lim, T.S. Su, T.Y. Hsieh, P.C. Lo, T.C. Wei, Beyond langevin recombination: how equilibrium between free carriers and charge transfer states determines the open- circuit voltage of organic solar cells, *Adv. Energy. Mater.* (2017) 1700169. <https://doi.org/10.1002/aenm.201500123>.
- [19] C.B. Gao, Y.X. Hu, M.S. Wang, M.F. Chi, Y.D. Yin, Fully alloyed Ag/Au nanospheres: combining the plasmonic property of Ag with the stability of Au, *J. Am. Chem. Soc.* 136 (2014) 7474–7479. <https://pubs.acs.org/doi/abs/10.1021/ja502890c>.
- [20] D.Q. Zhang, M.C. Wen, S.S. Zhang, P.J. Liu, W. Zhu, Au nanoparticles enhanced rutile TiO₂ nanorod bundles with high visible-light photocatalytic performance for NO oxidation, *Appl. Catal. B: Environ.* 147 (2014) 610–616. <https://doi.org/10.1016/j.apcatb.2013.09.042>.

- [21] H.M. Chen, C.K. Chen, M. L. Tseng, P.C. Wu, C.M. Chang, L.C. Cheng, H.W. Huang, T.S. Chan, D.W. Huang, R.S. Liu, D.P. Tsai, Plasmonic ZnO/Ag embedded structures as collecting layers for photogenerating electrons in solar hydrogen generation photoelectrodes, *Small* 17 (2013) 2926–2936. <https://doi.org/10.1002/sml.201202547>.
- [22] R. Solarska, K. Bienkowski, S. Zoladek, A. Majcher, T. Stefaniuk, P.J. Kulesza, J. Augustynski, Enhanced water splitting at thin tungsten trioxide photoanodes bearing plasmonic gold–polyoxometalate particles, *Angew. Chem. Int. Ed.* 53 (2014) 14196–14200. <https://doi.org/10.1002/anie.201408374>.
- [23] M. Valenti, D. Dolat, G. Biskos, A. Schmidt-Ott, W.A. Smith, Enhancement of the photoelectrochemical performance of CuWO₄ thin films for solar water splitting by plasmonic nanoparticle functionalization, *J. Phys. Chem. C* 119 (2015) 2096–2104. <https://pubs.acs.org/doi/abs/10.1021/jp506349t>.
- [24] H. Wang, T.T. You, W.W. Shi, J.H. Li, L. Guo, Au/TiO₂/Au as a plasmonic coupling photocatalyst, *J. Phys. Chem. C* 116 (2012) 6490–6494. <https://pubs.acs.org/doi/abs/10.1021/jp212303q>.
- [25] H. Zhang, J.M. Cai, Y.T. Wang, M.Q. Wu, M. Meng, Y. Tian, X.G. Li, J. Zhang, L.R. Zheng, Z. Jiang, J.L. Gong, Insights into the effects of surface/bulk defects on photocatalytic hydrogen evolution over TiO₂ with exposed {001} facets, *Appl. Catal. B: Environ.* 220 (2018) 126–136.

<https://doi.org/10.1016/j.apcatb.2017.08.046>.

[26] J.L. Li, M. Zhang, Z.J. Guan, Q.Y. Li, C.Q. He, J.J. Yang, *Appl. Catal. B: Environ.* 206 (2017) 300–307.

<https://doi.org/10.1016/j.apcatb.2017.01.025>.

[27] S. Kamimura, S. Yamashita, S. Abe, T. Tsubota, T. Ohno, Effect of core@shell (Au@Ag) nanostructure on surface plasmon-induced photocatalytic activity under visible light irradiation, *Appl. Catal. B: Environ.* 211 (2017) 11–17. <https://doi.org/10.1016/j.apcatb.2017.04.028>.

[28] M. Ou, S.P. Wan, Q. Zhong, S.L. Zhang, Y. Song, L.N. Guo, W. Cai, Y.L. Xu, Hierarchical Z-scheme photocatalyst of g-C₃N₄@Ag/BiVO₄(040) with enhanced visible-light-induced photocatalytic oxidation performance, *Appl. Catal. B: Environ.* 221 (2018) 97–107. <https://doi.org/10.1016/j.apcatb.2017.09.005>.

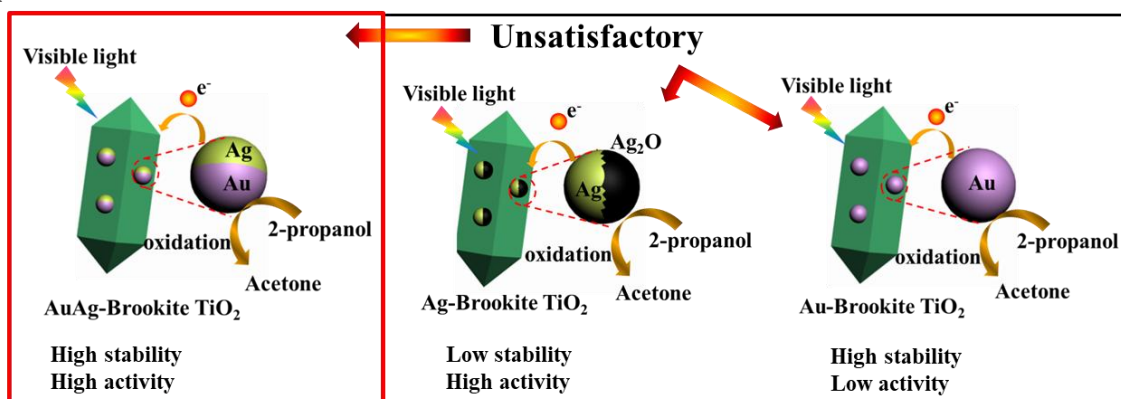
[29] N. Zhou, L. Polavarapu, N. Gao, Y.L. Pan, P.Y. Yuan, Q. Wang, Q.H. Xu, TiO₂ coated Au/Ag nanorods with enhanced photocatalytic activity under visible light irradiation, *Nanoscale* 5 (2013) 4236–4241. <https://pubs.rsc.org/en/content/articlelanding/2013/nr/c3nr00517h>.

[30] A. Tanaka, K. Hashimoto, H. Kominami, A very simple method for the preparation of Au/TiO₂ plasmonic photocatalysts working under irradiation of visible light in the range of 600–700 nm, *Chem. Commun.* 53 (2017) 4759–4762.

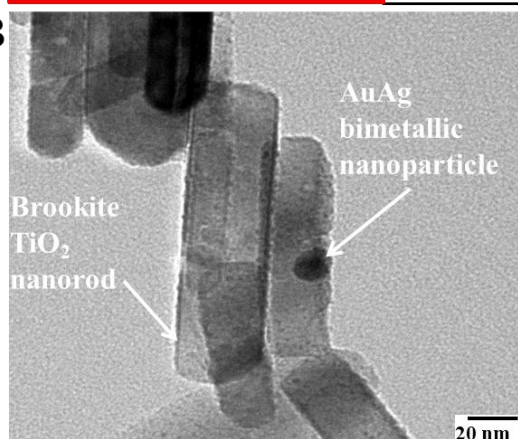
<https://pubs.rsc.org/en/content/articlelanding/2017/cc/c7cc01444a>.

- [31] L.G. Devi, B. Nagaraj, K.E. Rajashekhar, Synergistic effect of Ag deposition and nitrogen doping in TiO₂ for the degradation of phenol under solar irradiation in presence of electron acceptor, *Chem. Eng. J.* 181-182 (2012) 259–266. <https://doi.org/10.1016/j.cej.2011.11.076>.
- [32] T. Harifi, M. Montazer, Fe³⁺:Ag/TiO₂ nanocomposite: Synthesis, characterization and photocatalytic activity under UV and visible light irradiation, *Appl. Catal. A: Gen.* 473 (2014) 104–115. <https://doi.org/10.1016/j.apcata.2014.01.005>.
- [33] A. Tanaka, K. Hashimoto, H. Kominami, Control of surface plasmon resonance of Au/SnO₂ by modification with Ag and Cu for photoinduced reactions under visible- light irradiation over a wide range, *Chem. Eur. J* 22 (2016) 4592–4599. <https://doi.org/10.1002/chem.201504606>.
- [34] H. Li, Y. Sun, Z.Y. Yuan, Y.P. Zhu, T.Y. Ma, Titanium phosphonate based metal–organic frameworks with hierarchical porosity for enhanced photocatalytic hydrogen evolution, *Angew. Chem. Int. Ed.* 57 (2018) 3222–3227. <https://doi.org/10.1002/anie.201712925>.
- [35] N. Shao, J.N. Wang, D.D. Wang, P. Corvini, Preparation of three-dimensional Ag₃PO₄/TiO₂@MoS₂ for enhanced visible-light photocatalytic activity and anti-photocorrosion, *Appl. Catal. B: Environ.* 203 (2017) 984–978. <https://doi.org/10.1016/j.apcatb.2016.11.008>.

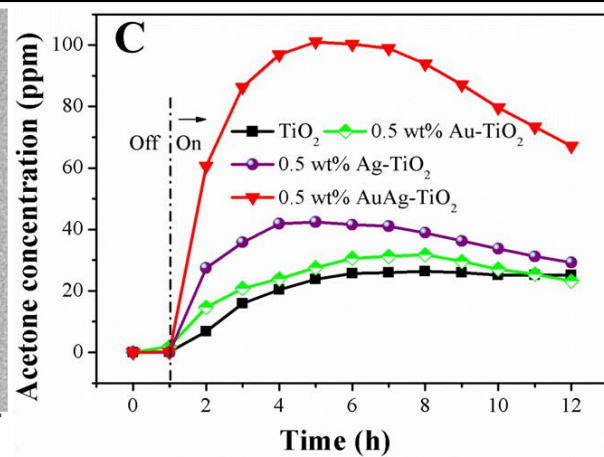
A



B



C



Brookite TiO₂ nanorods loaded with AuAg bimetallic nanoparticles are fabricated.

AuAg nanoparticles provide good stability and high surface plasmon resonance effect.

AuAg-TiO₂ shows higher photocatalytic performance than that of Au-TiO₂ and Ag-TiO₂.

AuAg-TiO₂ exhibits acetone production of 102 ppm under visible light irradiation.